Jin-yan Li*, Mei Zhang, Min Guo* and Xue-min Yang

Kinetic Study on Phosphate Enrichment Behavior in $CaO–SiO_2–FeO–Fe_2O_3–P_2O_5$ Steelmaking Slags

DOI 10.1515/htmp-2016-0241
Received November 27, 2016; accepted March 11, 2017

Abstract: The iso-thermal crystallization behavior of phosphate-enriched phase has been experimentally investigated in the rapidly quenched $CaO–SiO_2–FeO–Fe_2O_3–P_2O_5$ steelmaking slags under different cooling schedules. The experimental results indicate that increasing endpoint temperature from 1453 to 1533 K and prolonging holding time from 2 to 60 min can result in an increasing tendency of the size of phosphate-enriched phase in the shape of one-dimensional rod. The crystallization kinetics of phosphate-enriched phase in steelmaking slags has been described by Avrami equation. The Avrami constant n was obtained to be 0.472, while the crystallization rate constant k was recommended as $\ln k = 57.40 + 12,273.96/T - 8.25 \ln T - 5.5 \times 10^{-3} T$. Thus, the apparent activation energy E of crystallization is recommended as $E = 537.60 - 206.015T$ kJ/mol.

Keywords: phosphate enrichment, crystallization kinetics, steelmaking slags, apparent activation energy

Introduction

Steelmaking slags essentially containing more or less content of phosphate cannot be effectively utilized in the traditional metallurgical refining routes. As one of prospective techniques, the crystallization and selective enrichment of phosphate from steelmaking slags has been attached more attention in recent decade. From the viewpoint of thermodynamics, the phosphate enrichment process can be described in sequence as follows: (1) component P_2O_5 can be easily bonded by CaO to form tricalcium phosphate $3CaO{\cdot}P_2O_5$ (C_3P) [1–3], and the formed complex component C_3P can react with the produced dicalcium silicate $2CaO{\cdot}SiO_2$ (C_2S) to generate phosphate-enriched phase of solid solution $n2CaO{\cdot}SiO_2–3CaO{\cdot}P_2O_5$ ($nC_2S–C_3P$) [4] under the fixed cooling conditions; (2) acidic or amphoteric oxides or components containing aluminum [5–7], titanium [8,9], and fluorine [10] can indirectly affect phosphate enrichment behavior by combining with C_2S in steelmaking slags, i. e., the generated free C_2S content affects content of P_2O_5 of phosphate-enriched phase $nC_2S–C_3P$ in steelmaking slags; (3) the maximum content of P_2O_5 in $nC_2S–C_3P$ solid solution can reach to about 30.0 % [11]. On the other hand, the phosphate crystallization kinetics had also been investigated from the viewpoint of the influence of components in slags and crystallization temperature or endpoint temperature on viscosity [6, 9, 12], structure [6, 9, 12], and phosphorus distribution ratio [13, 14].

It is well known that the crystallization rate constant k related with apparent activation energy E of phosphate crystallization process is closely decided by cooling schedule including cooling rate, endpoint temperature, holding time and so on. The effect of cooling schedule on crystallization rate constant k of phosphate crystallization process in simple slags was studied through thermal analysis by single hot thermocouple technique (SHTT) [8, 15]. However, the crystallization kinetics of phosphate-enriched phase in complex steelmaking slags was usually studied by scanning electron microscopy (SEM) for detecting the mineralogical phases in quenched slag samples.

In this study, the mineralogical phases in the rapidly quenched slag samples of $CaO–SiO_2–FeO–Fe_2O_3–P_2O_5$ slag systems [11] have been detected by the SEM observation. Meanwhile, the average crystal area fraction of phosphate-enriched phase in the SEM images has been counted through the image manipulation software Image-Pro-Plus (IPP). The influence of endpoint temperatures and holding time on the average crystal area fraction of phosphate-enriched phase has been described by Avrami equation coupled with the optimized expression of

***Corresponding authors: Jin-yan Li,** Formerly School of Metallurgical and Ecological Engineering, University of Science and Technology Beijing, Beijing 100083, P. R. China; Now at China Metallurgical Industry Planning and Research Institute, Beijing 100711, P. R. China, E-mail: lijinyan0359@163.com
Min Guo, School of Metallurgical and Ecological Engineering, University of Science and Technology Beijing, Beijing 100083, P. R. China, E-mail: guomin@ustb.edu.cn
Mei Zhang, School of Metallurgical and Ecological Engineering, University of Science and Technology Beijing, Beijing 100083, P. R. China, E-mail: zhangmei@ustb.edu.cn
Xue-min Yang, Key Laboratory of Green Process and Engineering, Institute of Process Engineering, Chinese Academy of Sciences, Beijing 100190, P. R. China, E-mail: yangxm71@ipe.ac.cn

crystallization rate constant k through evaluating seven formulas of k from the literature. The kinetic behavior of phosphate-enriched phase in the steelmaking slags has been quantitatively described and predicted, meanwhile the optimal parameters of cooling schedule including endpoint temperatures, holding time, and cooling rate for obtaining larger size phosphate-enriched phase have been recommended.

Experimental

Experimental procedures

The $CaO–SiO_2–FeO–Fe_2O_3–P_2O_5$ slag system was applied to model the complex steelmaking slags through melting the prepared powders of ferrous oxide FeO and reagent-grade powders of CaO, SiO_2, Fe_2O_3, and P_2O_5, which reported in details by the present authors elsewhere [11]. The slag samples were synthesized in chemical composition of (% CaO) = 34.18, (% SiO_2) = 26.29, (% FeO) = 15.54, (% Fe_2O_3) = 26.29, and (% P_2O_5) = 5.00. The designed heating and cooling operations were conducted in a vertical tube-type heating furnace in ± 3 K fluctuation with $MoSi_2$ rods as heating elements. The high purity argon gas in 99.999 vol. % was used as carrier gas at a flow rate of 0.4 NL/min for avoiding re-oxidization of the prepared powders of ferrous oxide FeO during heating and cooling stages in all test-run experiments. In order to completely melt down the slag samples, 1773 K was applied to be the maximal heating temperature through heating the slag samples from ambient temperature at a rate of 3.0–5.0 K/min in Ar atmosphere.

From the standpoint of cooling schedule, two-group experiments were conducted in this study as listed in Table 1. In the first group of experiments, five test-run experiments corresponding to No. 1 to No. 5 in Table 1 were conduced to investigate the influence of endpoint temperature and holding time on kinetics of phosphate enrichment in the quenched slag samples at a fixed cooling rate of 5 K/min. Five endpoint temperatures at 1453, 1473, 1493, 1513, and 1533 K and four holding times in 2, 10, 30, and 60 min were applied as shown in Figure 1. In the second group of experiments, three test-run experiments corresponding to No. 6 to No. 8 in Table 1 were carried out at the endpoint temperature of 1453 K with holding time in 60 min at three cooling rates of 1, 3, and 5 K/min.

Two methods were adopted to take the slag samples in terms of holding time. The slag samples in Pt crucible in holding time less than 30 min were taken by quickly dipping a steel rod, while the slag samples in holding time longer than 30 min were taken by rapidly removing the Pt crucible from the furnace. The slag samples taken by dipping a steel rod or by removing Pt crucible were quenched by water. The water quenched slag samples were dried in an oven at 403 K for at least 4 hours.

In order to observe the micromorphology of quenched slag samples, the dried slag samples were mounted in epoxy resin, ground with SiC sandpapers, polished, and coated with carbon for the SEM (MLA250) observation. The phosphate enrichment area in crystalline phase was counted by the image manipulation software IPP. Thus, the crystalline area fraction of phosphate-enriched phase was experimentally determined for kinetic study.

Determination of endpoint temperature range

The possibly formed components in the steelmaking slags were calculated by FactSage 6.3 software over a temperature range from 1300 to 2000 K as shown in Figure 2. It can be observed in Figure 2 that the melting point of the slags is about 1560 K. The possibly formed components in the slags change in six temperature ranges: (1) In the case of $T > 1591$ K, the main components of the molten slags exist as simple oxides CaO, SiO_2, FeO, and Fe_2O_3, whereas P_2O_5 exist as solid solution C_3P. (2) In the case of $T < 1591$ K, iron oxides of both FeO and Fe_2O_3 tend to decrease and form Fe_3O_4. (3) In the case of $T < 1560$ K, simple oxides of CaO, SiO_2, FeO, and Fe_2O_3 show a decreasing tendency and solid solution $CaO{\cdot}SiO_2$ (CS) will be precipitated, while solid solution $3CaO{\cdot}2SiO_2$ (C_3S_2) will be also precipitated at $T < 1540$ K. (4) The simple oxides CaO, SiO_2, FeO, Fe_2O_3 will disappear at melting point as $T = 1560$ K. (5) In the case of $T < 1469$ K, the precipitations of Fe_3O_4, CS and C_3S_2 reach to their peaks, and solid solution $CaFeSiO_4$ is formed. (6) In the case of $T < 1439$ K, the solid solution C_3S_2 phase will decrease and CS phase can disappear.

Thus, the lowest crystallization temperature or endpoint temperature for the steelmaking slags was recommended over a temperature range from 1439 to 1540 K for the purpose of precipitating enough amount of C_2S phase.

Table 1: Determined crystallization area fraction of phosphate-enriched phase of eight test-run experiments and average grain diameters of No. 6–No. 8 test-run experiments under various cooling conditions.

Test No.	Endpoint temperature (K)	Crystallization area fraction of phosphate-enriched phase at various holding times (%)				Cooling rate (K/min)	Average grain diameter (μm)
		$t = 2$ min	$t = 10$ min	$t = 30$ min	$t = 60$ min		
1	1453	14.55	22.12	24.19	25.57	5	–
2	1473	13.07	19.50	23.72	25.41	5	–
3	1493	11.74	17.52	22.29	24.83	5	–
4	1513	8.75	13.53	20.02	24.79	5	–
5	1533	6.20	10.27	17.25	24.94	5	–
6	1453	–	–	–	26.17	1	64.7
7	1453	–	–	–	24.73	3	43.2
8	1453	–	–	–	25.57	5	37.8

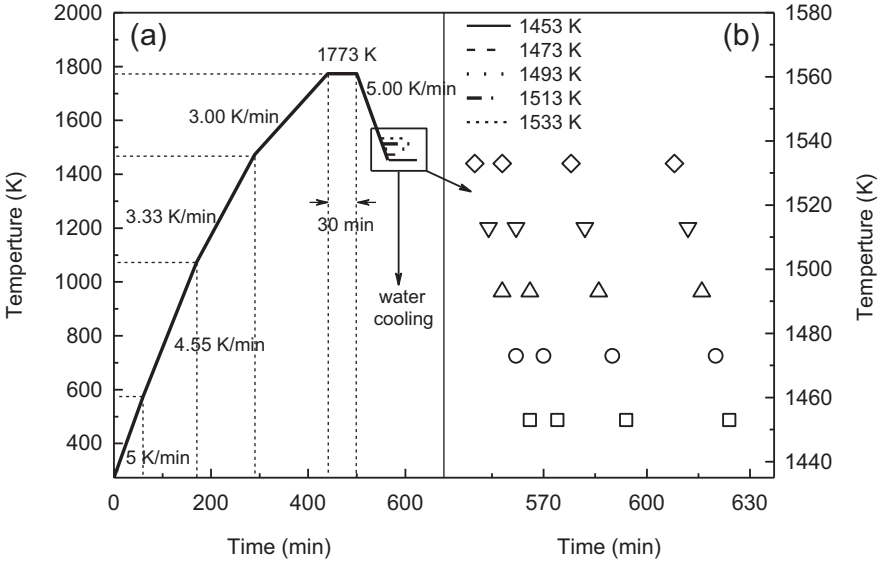

Figure 1: Applied heating schedule from ambient temperature to 1773 K and cooling schedule for slag samples of No. 1 to No. 5 test-run experiments.

Kinetic considerations of crystallization

It has been widely accepted that the iso-thermal crystallization kinetics of crystals can be quantitatively described by Avrami equation [16–19] as

$$x = 1 - \exp(-k \cdot t^n) \qquad (-) \qquad (1)$$

where x is the average mass fraction of formed crystals (–), k is the crystallization rate constant related with temperature (s^{-1}), t is the crystallization time (s), n is Avrami constant coupled with crystallization mechanism. Avrami equation [16–19] in eq. (1) can be rewritten through double-logarithmic transformation as

$$\ln[-\ln(1-x)] = n \ln t + \ln k \qquad (-) \qquad (2)$$

Evidently, Avrami constant n can be obtained from slope of the linear relationship between $\ln[-\ln(1-x)]$ and $\ln t$, while the crystallization rate constant $\ln k$ corresponds to the intercept. The relationship between Avrami constant n in eq. (1) and eq. (2) and crystallization mechanism can be correlated by [20, 21]

$$n = a + bc \qquad (-) \qquad (3)$$

where a means the crystal nucleation parameter (–), b stands for the crystal growth dimension parameter (–), and c is the crystal growth parameter (–). Three cases were defined [20, 21] to set the value of a as: (1) $a = 0$ was applied for the case with the crystallization rate

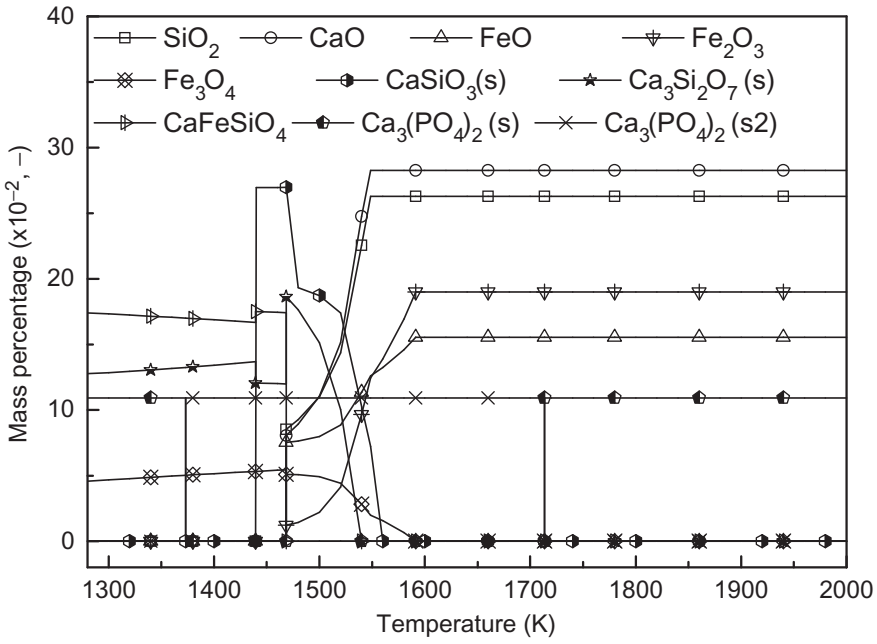

Figure 2: Variation of possibly formed components in $CaO–SiO_2–FeO–Fe_2O_3–P_2O_5$ steelmaking slags over a temperature from 1300 to 2000 K by FactSage software.

as zero; (2) $0 < a < 1$ was used for the case with the crystallization rate decreasing over prolonging crystallization time; and (3) $a > 1$ was applied for the case with the crystallization rate increasing over prolonging crystallization time. Similarly, three cases were also defined [20, 21] to set the value of b as $b = 1, 2, 3$ for the cases with one-dimension, two-dimension and three-dimension growth of crystalline phase, respectively. Meanwhile, there were two cases for setting the value of c as [20, 21]: (1) $c = 1$ was for the case of crystallization process controlled by the interface reaction; and (2) $c = 0.5$ was for the case of crystallization process controlled by phase diffusion.

The involved crystallization rate constant k in eq. (1) or eq. (2) of Avrami equation can be described by the famous Arrhenius formula as [22]

$$k = A\exp(-E/RT) \qquad (\mathrm{s}^{-1}) \qquad (4)$$

where A is the pre-exponential factor (–), E is the apparent activation energy of crystallization (J/mol), R is the gas constant (8.314 J/(mol·K)), and T is the endpoint temperature in this study (K). Obviously, Arrhenius formula in eq. (4) can be rewritten through logarithmic transformation as

$$\ln k = \ln A - E/RT \qquad (\mathrm{s}^{-1}) \qquad (5)$$

According to the linear relationship between $\ln k$ and $1/T$, the apparent activation energy E of crystallization can be obtained from the slope.

Beside the famous Arrhenius formula in eq. (4) or eq. (5), some formulas claimed as non-Arrhenius formulas were also proposed as listed in the second column of Table 2. Clearly, six collected formulas of non-Arrhenius formulas are named as M2–M7, while Arrhenius formula in eq. (4) or eq. (5) is labeled as M1.

The formula M2 by Harcourt–Esson [23] was applied by Dollimore et al. [24] to interpret the decomposition kinetics of calcium carbonate ($CaCO_3$). The formula M3 by Berthelot–Hood [25, 26] was used by Simon [27]. Beside formula M4 by Kooij [28] as well as formulas M5 and M7 by van't Hoff [29] originally developed in the nineteenth century, formula M6 was proposed by Flynn [30] in 1997. It is interesting to find that all seven collected formulas from M1 to M7 can be expressed in a general form as $\ln k = \ln A - j_1/T + j_2 \ln T + j_3 T$.

The apparent activation energy E of crystallization for seven formulas in Table 2 can be derived as

$$E = -R\frac{\mathrm{d}\ln k}{\mathrm{d}(1/T)} = RT^2\frac{\mathrm{d}\ln k}{\mathrm{d}T} \qquad (\mathrm{J/mol}) \qquad (6)$$

Thus, seven formulas in the second column of Table 2 can be also expressed in natural logarithmic forms as listed in the third column. The derived formulas of the apparent activation energy E of crystallization from eq. (6) are summarized in the fifth column of Table 2 combining with the formulas of $\mathrm{d}\ln k/\mathrm{d}T$ in the fourth column.

Table 2: Summary of seven collected formulas of crystallization rate constant k from the literature.

Formula No.	Formula of k (s^{-1})	Expression of ln k (s^{-1})	$d(\ln k)/dT$ ($s^{-1}\cdot K^{-1}$)	Expression of E (J/mol)	Author(s)	Ref.
M1	$k = A\exp(-E/RT)$	$\ln k = \ln A - E/RT$	$1/(RT^2)$	E	Arrhennius	[22]
M2	$k = AT^{j_2}$	$\ln k = \ln A + j_2 \ln T$	j_2/T	Rj_2T	Harecourt and Esson	[23]
M3	$k = A\exp(j_3T)$	$\ln k = \ln A + j_3T$	j_3	Rj_3T^2	Berthelot and Hood	[25, 26]
M4	$k = AT^{j_2}\exp(-j_1/T)$	$\ln k = \ln A - j_1/T + j_2 \ln T$	$j_1/T^2 + j_2/T$	$R(j_1 + j_2T)$	Kooij	[28]
M5	$k = A\exp(j_3T)\exp(-j_1/T)$	$\ln k = \ln A - j_1/T + j_3T$	$j_1/T^2 + j_3$	$R(j_1 + j_3T^2)$	van't Hoff	[29]
M6	$k = AT^{j_2}\exp(j_3T)$	$\ln k = \ln A + j_2 \ln T + j_3T$	$j_2/T + j_3$	$R(j_2T + j_3T^2)$	Flynn	[30]
M7	$k = AT^{j_2}\exp(j_3T)\exp(-j_1/T)$	$\ln k = \ln A - j_1/T + j_2 \ln T + j_3T$	$j_1/T^2 + j_2/T + j_3$	$R(j_1 + j_2T + j_3T^2)$	van't Hoff	[29]

Results and discussion

Determination of crystallization area fraction

The SEM images for slag samples of No. 1, No. 3, and No. 5 test-run experiments at three endpoint temperatures in four holding times are displayed in Figure 3. Taking slag sample of No. 1 test-run experiment as an example, the SEM images of No. 1 slag samples in four holding times of 2, 10, 30, and 60 min are shown in Figures 3(a1)–3(a4). The similar labels are also used to No. 3 and No. 5 slag samples in Figures 3(b1)–3(b4) and 3(c1)–3(c4), respectively. Three zones in white, gray, and dark color can be observed in Figure 3, whereas the white zone is iron oxides-enriched phase, the gray zone is matrix phase and the dark zone is phosphate-enriched phase, which is the same as those reported in the previous study [5].

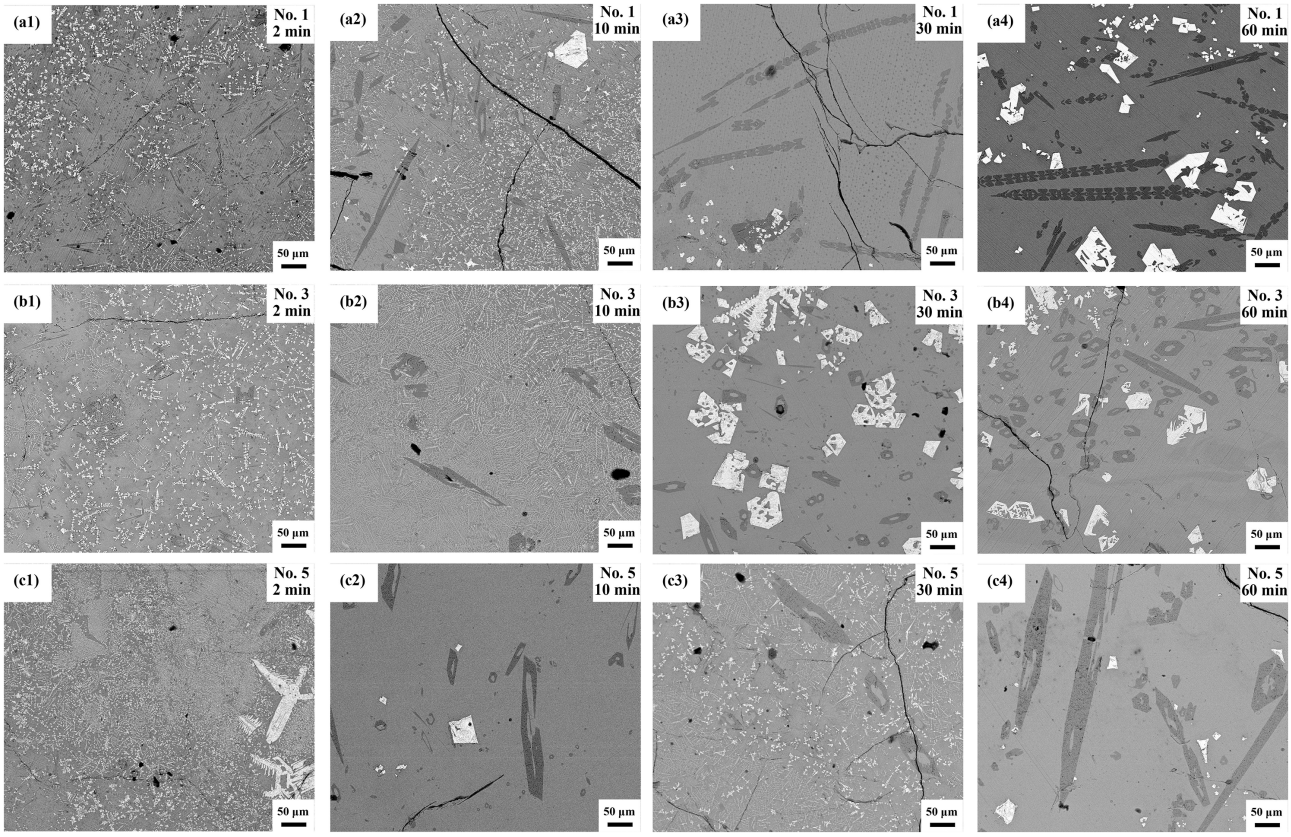

Figure 3: SEM images of No. 1, No. 3 and No. 5 test-run slag samples at three endpoint temperatures of 1453 K (a), 1493 K (b), and 1533 K (c) with four holding times in 2, 10, 30, 60 min, respectively.

It can be confirmed from Figure 3 that increasing the endpoint temperature and prolonging the holding time can result in an increasing tendency of the size of phosphate-enriched phase in dark zones. In comparison with the SEM images in Figures 3(a1)–3(a4), it can be deduced that increasing the holding time at the fixed endpoint temperature of 1453 K can promote the size of phosphate-enriched phase in dark zones. Thus, prolonging the holding time is an effective measure to expand the size of phosphate-enriched phase.

In comparison with the SEM images in Figures 3(a1), 3(b1), and 3(c1), it can be deduced that increasing the endpoint temperature from 1453 to 1513 K can promote the formation of phosphate-enriched phase in dark zones in the same holding time of 2 min. It is due to that improving the endpoint temperature can decrease the instantaneous nucleation numbers, thus increase the size of phosphate-enriched phase in dark zones. It is further verified through comparing with Figures 3(a4), 3(b4), and 3(c4) that the phosphate-enriched phase in dark zones can be increased with improving the endpoint temperature in the fixed holding time of 60 min because of enhancing diffusion of phosphate-enriched phase.

The measured results of crystallization area fraction of phosphate-enriched phase in dark zones for all 20 quenched slag samples from the SEM images by software IPP are summarized in Table 1. The crystallization mass fraction x is proportional to the measured area ratio of phosphate-enriched phase in dark zones to the total slag samples. Thus, it can be replaced by the measured area ratio of formed phosphate-enriched phase in the SEM images as suggested by Ito et al. [31]

The influence of holding time on the average crystallization area fraction as well as the normalized area fraction of phosphate-enriched phase at five endpoint temperatures is illustrated in Figures 4(a) and 4(b), respectively. It can be observed in Figure 4 that prolonging the holding time can result in an increasing tendency of the average crystal area fraction as well as the normalized area fraction of phosphate-enriched phase. The average crystal area fraction of phosphate-enriched phase can reach to the maximum value as 25.57 % at five endpoint temperatures through prolonging the holding time to 60 min.

Kinetic description of phosphate-enriched phase in steelmaking slags

In order to describe the iso-thermal crystallization kinetics of phosphate-enriched phase by Avrami equation in eq. (1) or eq. (2), the involved parameters such as Avrami constant n and crystallization rate constant k should be in first determined.

Determination of Avrami constant *n*

The relationship between $\ln t$ and $\ln[-\ln(1-x)]$ at five endpoint temperatures is shown in Figure 5, respectively. The obtained Avrami constant n and crystallization rate constant $\ln k$ from the regressed slopes and intercepts of linear plots in Figure 5 are tabulated in Table 3. It should be emphasized that the unit of holding time in Figure 5 must be in second, rather than in minute. Otherwise,

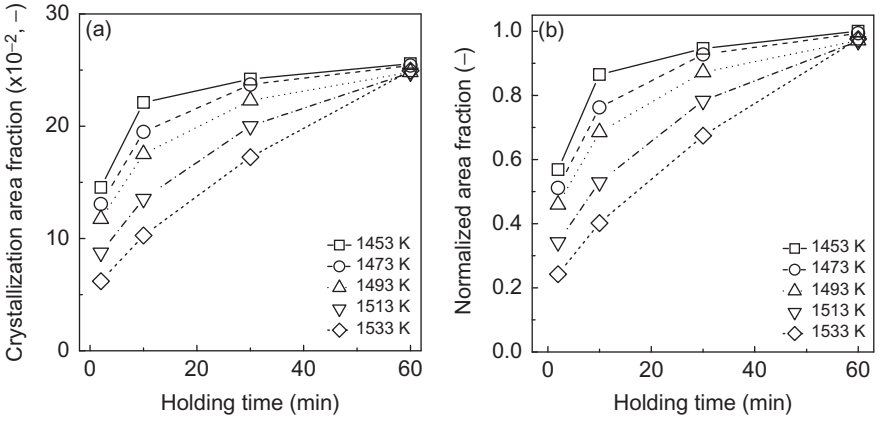

Figure 4: Influence of holding time on crystallization area fraction (a) and normalized area fraction (b) of phosphate-enriched phase in $CaO–SiO_2–FeO–Fe_2O_3–P_2O_5$ steelmaking slags over a temperature range from 1453 to 1533 K, respectively.

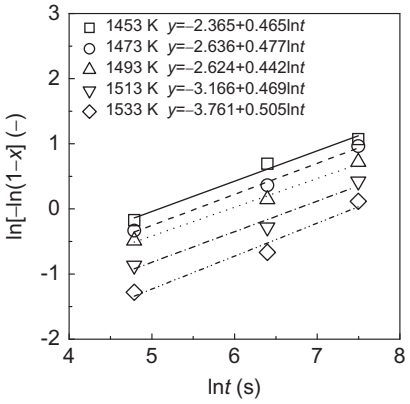

Figure 5: Relationship between holding time in natural logarithmic form $\ln t$ and $\ln[-\ln(1-x)]$ for phosphate-enriched phase in CaO–SiO_2–FeO–Fe_2O_3–P_2O_5 steelmaking slags at temperatures of 1453, 1473, 1493, 1513 and 1533 K, respectively.

Table 3: Obtained results of Avrami constant n and crystallization rate constant $\ln k$ of phosphate-enriched phase in steelmaking slags at five endpoint temperatures.

Test No.	Endpoint temperature (K)	Avrami constant n (–)	$\ln k$ (s^{-1})
1	1453	0.465	–2.365
2	1473	0.477	–2.637
3	1493	0.442	–2.624
4	1513	0.469	–3.166
5	1533	0.506	–3.761

wrong results of slopes and intercepts will be produced. The obtained Avrami constant n changes from 0.442 to 0.506 with an average in 0.472.

It was reported [32, 33] that the phosphate-enriched phase crystallization was controlled by phase diffusion. Thus, the crystallization growth parameter c should be set as $c = 0.5$. Furthermore, the observed phosphate-enriched phase is in the shape of one-dimensional rod as shown in Figure 3, the crystallization growth dimension parameter b is set as $b = 1$. According to the relationship of $n = a + bc$ in eq. (3), the crystallization nucleation parameter a should be set as $a < 1$ under conditions of $b = 1$, $c = 0.5$, and $n = 0.472$. This result conforms to the definition of crystallization nucleation parameter $0 < a < 1$ introduced in section "Kinetic considerations of crystallization" as that the crystallizing rate of phosphate-enriched phase decreases with an increase of holding time.

Optimization of formula of crystallization rate constant k and determination of apparent activation energy E

Seven formulas of crystallization rate constant k as listed in Table 2 were used to determine the apparent activation energy E of crystallization. Based on the results of E with less errors, the optimal formula of crystallization rate constant k is recommended.

The relationship between $\ln k$ and $1/T$ by formula M1 in Table 2 is illustrated in Figure 6(a). The apparent activation energy E of crystallization for phosphate-enriched phase can be determined as $E = -306.137$ kJ/mol from the slope, i. e., E/R, as 36.821 in Figure 6(a). Meanwhile, the relationship of $\ln k$ against T by formula M2 or against $\ln T$ by formula M3 is displayed in Figures 6(b) and 6(c), respectively. Obviously, the slopes of the regressed linear plots give adjustable parameters j_2 and j_3. Thus, the apparent activation energy E by formulas M2 and M3 can be calculated by the formulas in the fifth column in Table 2. The calculated results of E by formulas M2 and M3 at five endpoint temperatures are listed in Table 4.

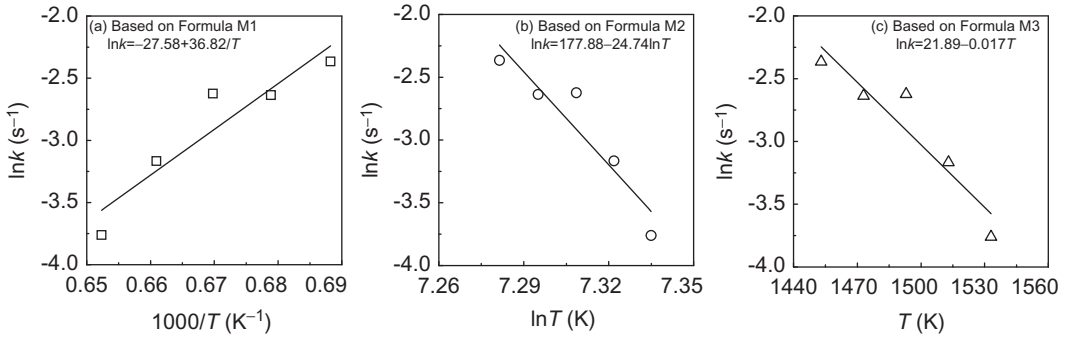

Figure 6: Relationship of crystallization rate constant in natural logarithmic form $\ln k$ by three formulas of k against $1/T$ (a) or $\ln T$ (b) or endpoint temperature T (c) over a temperature range from 1453 to 1533 K, respectively.

Table 4: Regressed results of pre-exponential factor ln A, adjustable parameters j_1, j_2, and j_3, apparent activation energy E of crystallization, and mean deviation δ_E based on seven collected formulas of k.

Formula No.	Regressed results of parameters in expression of k in form of $\ln k = \ln A - j_1/T + j_2 \ln T + j_3 T$				Apparent activation energy E at five endpoint temperatures (J/mol)					Mean deviation δ_E ($\times 10^{-2}$, –)
	Pre-exponential factor ln A (–)	Adjustable parameters								
		j_1 (–)	j_2 (–)	j_3 (–)	T = 1453 K	T = 1473 K	T = 1493 K	T = 1513 K	T = 1533 K	
M1	−27.58	−36,821.87	–	–	−306,137	−306,137	−306,137	−306,137	−306,137	−1.66
M2	177.88	–	−24.74	–	−298,834	−302,947	−307,060	−311,174	−315,287	−0.01
M3	21.89	–	–	−0.017	−291,548	−299,629	−307,821	−316,124	−324,536	−1.66
M4	75.150	−18,410.94	−12.37	–	−302,485	−304,542	−306,598	−308,655	−310,712	−0.83
M5	−2.84	−18,410.94	–	−0.0083	−298,842	−302,883	−306,979	−311,130	−315,336	−0.01
M6	99.89	–	−12.37	−0.0083	−295,191	−301,288	−307,441	−313,649	−319,912	−0.83
M7	57.40	−12,273.96	−8.25	−0.0055	−298,839	−302,904	−307,006	−311,145	−315,320	0.00
Average*	ND	ND	ND	ND	−298,840	−302,905	−307,007	−311,145	−315,320	ND

*Note: ND means no data.

To formulas M4–M7, the pre-exponential factor ln A and adjustable parameters j_1 of $1/T$, j_2 of $\ln T$, and j_3 of T can be also obtained through the multiple linear regression method based on the results of $\ln k$ at various endpoint temperatures T in different holding times. Thus, the apparent activation energy E of crystallization by four formulas of M4 to M7 can be determined by the expressions of E in the fifth column of Table 2 as listed in Table 4.

The effect of endpoint temperatures from 1453 to 1533 K on the obtained apparent activation energy E of crystallization by seven formulas of k in Table 4 is shown in Figure 7(a), respectively. Large discrepancies of the obtained apparent activation energy E of crystallization can be observed in Figure 7(a) by seven formulas of k. In order to find the best formula among seven formulas of k, the mean deviation of apparent activation energy δ_E is calculated based on the mean activation energy $E_{\text{Avg.}}$ as a basis through

$$\delta_E = \frac{1}{m}\sum\left(\frac{|E - E_{\text{Avg.}}|}{E_{\text{Avg.}}}\right) \times 100 \quad (-) \qquad (5)$$

where m is the number of slag samples as 5 (–). The means deviation of apparent activation energy δ_E by seven formulas is illustrated in Figure 7(b). It can be observed in Figures 7(a) and 7(b) that three formulas M2, M5 and M7 of k can produce smaller mean deviation δ_E comparing with the largest ones by formula M1. Thus, the crystallization rate constant $\ln k$ can be described as $\ln k = 57.40 + 12,273.96/T - 8.25 \ln T - 5.5 \times 10^{-3} T$ in the form of formula M7 of k. Meanwhile, the determined apparent activation energy E of crystallization can be expressed by $E = 537.60 - 206.015T$ kJ/mol based on formula M7 of k.

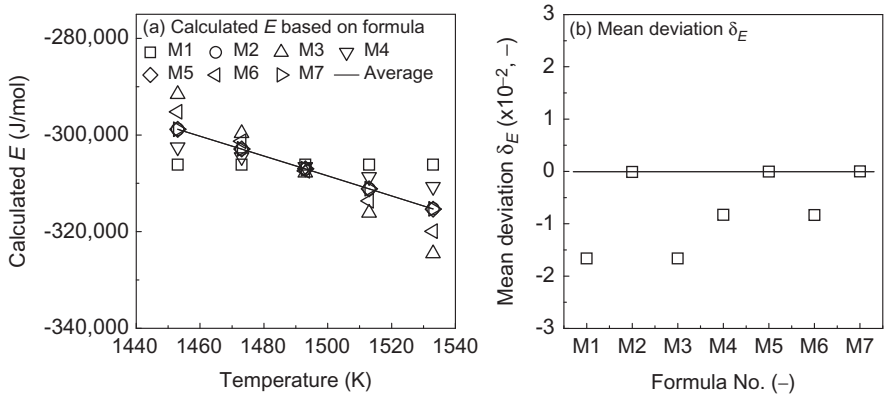

Figure 7: Comparison of calculated apparent activation energy E (a) and mean deviation δ_E (b) by seven collected formulas of k over a temperature range from 1453 to 1533 K, respectively.

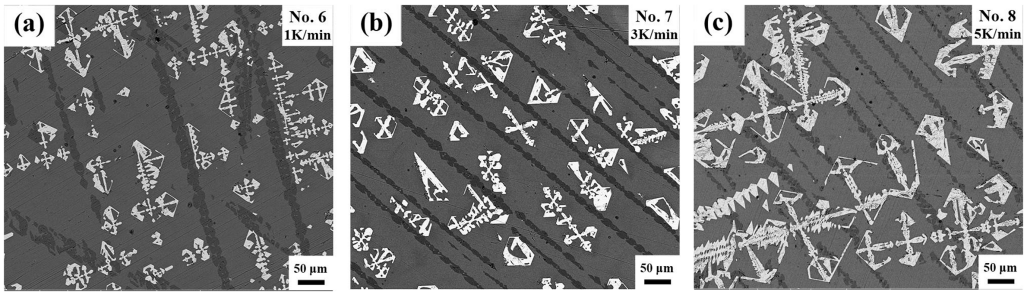

Figure 8: SEM images of No. 6 to No. 8 test-run slag samples under the condition of keeping endpoint temperature at 1453 K with holding time in 60 min at three cooling rates of 1, 3, and 5 K/min, respectively.

Effect of cooling rate on grain size of phosphate-enriched phase

The SEM images of the slag samples in the second group of experiments, i. e., No. 6–No. 8 test-run experiments, is displayed in Figure 8, respectively. The measured average crystal area fraction and grain size of phosphate-enriched phase in the slag samples of No. 6–No. 8 test-run experiments are also summarized in Table 1. It can be obtained from Table 1 that increasing cooling rate from 1 to 5 K/min can result in a decreasing tendency of the grain size of phosphate–enriched phase. Lower cooling rate can promote the formation of phosphate-enriched phase in larger size. Larger than 40 μm as a criterion size [32, 33] is beneficial to separating the formed phosphate-enriched phase in steelmaking slags. Thus, the cooling rate smaller than 3 K/min is recommended for easily separation phosphate-enriched phase from the quenched slag samples in terms of viewpoint of the crystallization and selective enrichment of phosphate.

Conclusions

The iso-thermal crystallization behavior of phosphate-enriched phase has been experimentally investigated in the rapidly quenched $CaO–SiO_2–FeO–Fe_2O_3–P_2O_5$ steelmaking slags under different cooling schedules. The crystallization kinetics has been described by Avrami equation including Avrami constant n and crystallization rate constant k. Furthermore, the apparent activation energy E of crystallization has also been determined based on evaluation of seven collected formulas of crystallization rate constant k. The main summary remarks can be summarized as follows:

(1) The obtained Avrami constant n from experimental results is 0.472 during crystallization of phosphate-enriched phase in steelmaking slags. The involved two parameters in Avrami constant n as the crystallization growth parameter c and the crystallization growth dimension parameter b can be set as 0.5 and 1.0, respectively. Thus, the crystallization nucleation parameter a is derived to be less than 1.0 according to the definition of Avrami constant $n = a + bc$. This means that the crystallizing rate of phosphate-enriched phase in steelmaking slags shows a decreasing trend with an increase of holding time.

(2) The apparent activation energy E of crystallization has been obtained by seven formulas of the crystallization rate constant k. The accurate results of apparent activation energy E of crystallization can be obtained by formulas M7 of k. The crystallization rate constant k is recommended as $\ln k = 57.40 + 12,273.96/T - 8.25 \ln T - 5.5 \times 10^{-3} T$, while the apparent activation energy E of crystallization is recommended as $E = 537.60 - 206.015T$ kJ/mol based on formula M7 of k.

(3) The phosphate-enriched phase greater than 40 μm in the shape of one-dimensional rod can be formed in the quenched slag samples at cooling rate smaller than 3 K/min from 1773 to 1453 K in holding time of 60 min.

Acknowledgments: The work was financially supported by the National Basic Research Program of China (No. 2014CB643401), the National Natural Science Foundation of China (Nos. 51372019, 51174186, and 51072022).

Funding: National Natural Science Foundation of China, (Grant / Award Number: 'Nos. 51372019, 51174186, and 51072022'.).

References

[1] R. Inoue and H. Suito, *ISIJ Int.*, 46 (2006) 174–179.
[2] H. Suito and R. Inoue, *ISIJ Int.*, 46 (2006) 180–187.
[3] R. Inoue and H. Suito, *ISIJ Int.*, 46 (2006) 188–194.
[4] W. Fix, H. Heyman and R. Heinke, *J. Am. Ceram. Soc.*, 52 (1969) 346–347.
[5] L. Lin, Y.P. Bao, M. Wang and H.M. Zhou, *Ironmaking Steelmaking*, 41 (2014) 193–198.
[6] Z.J. Wang, Y.Q. Sun, S. Sridhar, M. Zhang, M. Guo and Z.T. Zhang, *Metall. Mater. Trans. B*, 46B (2015) 537–541.
[7] Z.J. Wang, Y.Q. Sun, S. Sridhar, M. Zhang, M. Guo and Z.T. Zhang, *Metall. Mater. Trans. B*, 46B (2015) 2246–2254.
[8] J. Li, X.D. Wang and Z.T. Zhang, *ISIJ Int.*, 51 (2011) 1396–1402.
[9] Y.Q. Sun, K. Zheng, J.L. Liao, X.D. Wang and Z.T. Zhang, *ISIJ Int.*, 54 (2014) 1491–1497.
[10] Z.J. Wang, Y.Q. Sun, S. Sridhar, M. Zhang, M. Guo and Z.T. Zhang, *ISIJ Int.*, 56 (2016) 546–553.
[11] J.Y. Li, M. Zhang, M. Guo and X.M. Yang, *Int. J. Min. Met. Mater.*, 23 (2016) 520–533.
[12] Z.J. Wang, Q.F. Shu, S. Sridhar, M. Zhang, M. Guo and Z.T. Zhang, *Metall. Mater. Trans. B*, 46B (2015) 758–765.
[13] X. Gao, H. Matsuura, M. Miyata and F. Tsukihashi, *ISIJ Int.*, 53 (2013) 1381–1385.
[14] S.L. Xie, W.L. Wang, Y.Z. Liu and H. Matsuura, *ISIJ Int.*, 54 (2014) 766–773.
[15] K. Yoshiaki, C.E. Cicutti and A.W. Cramb, *ISIJ Int.*, 38 (1998) 357–365.
[16] M.C. Weinberg, D.P. Birnie III and V.A. Shneidman, *J. Non-Cryst. Solids*, 219 (1997) 89–99.
[17] P.N. Kalu and D.R. Waryoba, *Mat. Sci. Eng. A-Struct.*, 464 (2007) 68–75.
[18] J.J. Li, J.C. Wang, Q. Xu and G.C. Yang, *Acta Materialia*, 55 (2007) 825–832.
[19] A.T. Lorenzo, M.L. Arnal, J. Albuerne and A.J. Muller, *Polym. Test.*, 26 (2007) 222–231.
[20] S. Ranganathan and M.V. Heimendahl, *J. Mater. Sci.*, 16 (1981) 2401–2404.
[21] K. Matusita, T. Komatsu and R. Yokota, *J. Mater. Sci.*, 19 (1984) 291–296.
[22] S. Arrhenius, *Z. Physik Chem.*, 226 (1889) 23–26.
[23] A.V. Harecourt and W. Esson, *Proc. Roy. Soc.*, 58 (1895) 112.
[24] D. Dollimore, P. Tong and K.S. Alexander, *Thermochim. Acta*, 282/283 (1996) 13–27.
[25] M. Berthelot, *Ann. De Chim. Et De Phys.*, 366 (1862) 110–117.
[26] J.J. Hood, *Phil. Mag.*, 20 (1885) 323.
[27] P. Simon, *J. Therm. Anal. Calorim.*, 79 (2005) 703–708.
[28] D.M. Kooij, *Int. J. Res. Phys. Chem. Chem. Phys.*, 12 (1893) 155–161.
[29] J.H. *van't* Hoff, Lectures on Theoretical and Physical Chemistry, *Trans. R.A. Lechfeldt*, Edward Arnold Publisher: Oxford, London, Part 1, Chemical Dynamics (1899) 230–235.
[30] J.H. Flynn, *Thermochim. Acta*, 300 (1997) 83–92.
[31] K. Ito, M. Yanagisawa and N. Sano, *Tetsu–to–Hagané*, 68 (1982) 342–344.
[32] N. Wang, Z.G. Liang, M. Chen and Z.S. Zou, *J. Iron Steel Res. Int.*, 18 (2011) 17–19, 39.
[33] N. Wang, Z.G. Liang, M. Chen and Z.S. Zou, *J. Iron Steel Res. Int.*, 18 (2011) 22–26.